JASN

Spatiotemporal ATP dynamics during acute kidney injury predicts renal prognosis

Journal:	*Journal of the American Society of Nephrology*
Manuscript ID	JASN-2020-05-0580.R1
Manuscript Type:	Original Article - Basic Research
Date Submitted by the Author:	n/a
Keywords:	ATP, energy dynamics, imaging, AKI, fibrosis, hypothermia

Complete List of Authors:
Yamamoto, Shinya; Kyoto University, Department of Nephrology
Yamamoto, Masamichi; Kyoto University, Department of Nephrology
Nakamura, Jin; Kyoto University
Mii, Akiko; Nippon Medical School, Nephrology
Yamamoto, Shigenori; Kyoto University
Takahashi, Masahiro; Kyoto University, Department of Nephrology
Kaneko, Keiichi; Kyoto University
Uchino, Eiichiro; Graduate School of Medicine, Kyoto University, Nephrology;
Sato, Yuki; Kyoto University, Nephrology
Fukuma, Shingo; Kyoto University, Department of Healthcare Epidemiology
Imamura, Hiromi; Kyoto University
Matsuda, Michiyuki; Kyoto University
Yanagita, Motoko; Kyoto University, Department of Nephrology

Note: The following files were submitted by the author for peer review, but cannot be converted to PDF. You must view these files (e.g. movies) online.

Movie A PT ischemia.mp4
Movie A DT CD ischemia.mp4
Movie B w15 reperfusion.mp4
Movie B w30 reperfusion.mp4
Movie B w60 reperfusion.mp4
Movie C1 w15 dextran 5min.mp4
Movie C1 w30 dextran 5min.mp4
Movie C1 w60 dextran 5min.mp4
Movie C2 w60 dextran.mp4

Significance Statement

ATP depletion plays the central role in the pathogenesis of kidney diseases. Nevertheless, *in vivo* ATP dynamics in the kidney remained unclear due to technical difficulty. Using the novel mouse strain to visualize spatiotemporal ATP dynamics at single cell resolution, the authors revealed the crucial difference of ATP dynamics between proximal tubules and distal tubules, which were also supported by morphological changes of mitochondria, explaining the different sensitivity to ischemic reperfusion injury. The authors also showed the strong correlation between ATP recovery of proximal tubules in acute phase and renal fibrosis in chronic phase. Cold ischemia enhanced ATP recovery, providing a proof of concept for renal hypothermia. This powerful tool has improved our understanding of kidney energy dynamics.

Spatiotemporal ATP dynamics during acute kidney injury predicts renal prognosis

Shinya Yamamoto[1], Masamichi Yamamoto[1, 2, 3], Jin Nakamura[1#], Akiko Mii[1$], Shigenori Yamamoto[1], Masahiro Takahashi[1], Keiichi Kaneko[1], Eiichiro Uchino[1], Yuki Sato[1, 4], Shingo Fukuma[5], Hiromi Imamura[6], Michiyuki Matsuda[7], Motoko Yanagita[1, 8]

[1]Department of Nephrology, [4]Medical Innovation Center TMK Project, [5]Department of Human Health Sciences, [7]Department of Pathology and Biology of Diseases, Graduate School of Medicine, Kyoto University, Kyoto, Japan

[2]Advanced Scientific Research Leaders Development Unit, Gunma University Graduate School of Medicine

[3]PRESTO, Japan Science and Technology Agency (JST)

[6]Graduate School of Biostudies, Kyoto University, Kyoto, Japan

[8]Institute for the Advanced Study of Human Biology (WPI-ASHBi), Kyoto University, Kyoto, Japan

[#]The present address of Jin Nakamura is Deloitte Tohmatsu Consulting LLC, Tokyo, Japan

[$]The present address of Akiko Mii is Department of Nephrology, Nippon Medical School, Tokyo, Japan

[*]To whom correspondence should be addressed:

Motoko Yanagita: Department of Nephrology, Graduate School of Medicine, Kyoto University, Shogoin-Kawahara-cho 54, Sakyo-ku, Kyoto 606-8507, Japan.

E-mail: motoy@kuhp.kyoto-u.ac.jp, Tel: +81-75-751-3860, Fax: +81-75-751-3859

Significance Statement

ATP depletion plays the central role in the pathogenesis of kidney diseases. Nevertheless, *in vivo* ATP dynamics in the kidney remained unclear due to technical difficulty. Using the novel mouse strain to visualize spatiotemporal ATP dynamics at single cell resolution, the authors revealed the crucial difference of ATP dynamics between proximal tubules and distal tubules, which were also supported by morphological changes of mitochondria, explaining the different sensitivity to ischemic reperfusion injury. The authors also showed the strong correlation between ATP recovery of proximal tubules in acute phase and renal fibrosis in chronic phase. Cold ischemia enhanced ATP recovery, providing a proof of concept for renal hypothermia. This powerful tool has improved our understanding of kidney energy dynamics.

Abstract

Background Renal tubular cells constantly produce and consume ATP, of which depletion plays the central role in the pathogenesis of kidney diseases. Nevertheless, lack of technology to visualize *in vivo* ATP has hindered further analysis.

Methods We generated a novel mouse line expressing ATP biosensor systemically. We monitored spatiotemporal ATP dynamics at single cell resolution during both warm and cold ischemic reperfusion (IR) with two-photon microscopy. Furthermore, we performed the quantification of fibrosis two weeks after IR, and assessed the correlation between the ATP recovery in acute phase and fibrosis in chronic phase.

Results Upon ischemia induction, the ATP levels of proximal tubules (PTs) decreased to the nadir within a few minutes, whereas those of distal tubules (DTs) decreased gradually up to 1 hour. Upon reperfusion, the recovery rate of ATP in PTs was slower with longer ischemia. In stark contrast, ATP in DTs was quickly restored irrespective of ischemia duration. Different ATP dynamics in two segments were also supported by morphological changes of mitochondria in acute phase. Furthermore, the ATP recovery of PTs in acute phase inversely correlated with fibrosis in chronic phase. In addition, ischemia in hypothermia resulted in more rapid and complete ATP recovery with less fibrosis, providing a proof of concept for hypothermia to protect kidney.

Conclusions We succeeded in visualizing the spatiotemporal ATP dynamics during IR injury and revealed the higher sensitivity of PTs to ischemia in terms of energy metabolism. The ATP dynamics of PTs in acute phase might predict renal prognosis.

Introduction

Acute kidney injury (AKI) is a common clinical condition associated with high morbidity and mortality.[1, 2] Previous clinical studies demonstrate that AKI predisposes to the development and progression of chronic kidney disease (CKD),[3, 4] and the concept of AKI to CKD transition has been established, however, the underlying mechanisms of AKI to CKD transition remain unclear.[5] Recent studies indicate that the impaired renal energy metabolism and mitochondrial dysfunction are linked with AKI to CKD transition.[6-10]

Adenosine 5' triphosphate (ATP) is often referred to as the "molecular unit of currency" of intracellular energy transfer,[11] because of its key roles in energy metabolism. The kidney constantly requires a large amount of ATP to meet the demands for their intricate functions. Alteration of cellular ATP levels during ischemia and reperfusion was previously demonstrated utilizing luciferase assays and nuclear magnetic resonance spectroscopy of whole kidneys.[12-15] Several lines of evidence utilizing dissected nephrons indicate that ATP source in the kidney might be cell-type specific.[16-19] The proximal tubules (PTs), which consume ATP for reabsorption and are the vulnerable segment during ischemia,[20] are considered to depend mostly on mitochondrial oxidative phosphorylation for energy supply, while the distal tubules (DTs) are considered to have the potential to produce ATP by glycolysis.

Although this cell-type specificity might be one of the reasons explaining the vulnerability of PTs to ischemic insults than DTs,[21] ATP dynamics in each nephron segment during kidney injuries have been unknown because of lack of technology to visualize *in vivo* spatiotemporal ATP dynamics at a single cell level non-invasively. The conventional ATP quantification method utilizing luciferase assay does not allow us to monitor the spatiotemporal ATP dynamics in the tissues. Mass imaging technique provides us spatial distribution of ATP in the kidney sections, but not ATP dynamics during injury in native microenvironment, especially in the point of oxygen and substrate supply. To visualize ATP dynamics *in vivo*, we generated a

novel mouse line, which expresses the Förster resonance energy transfer (FRET)-based ATP biosensor[22] in all tissues.[23]

Here we, for the first time, demonstrate *in vivo* spatiotemporal ATP dynamics in the kidney at a single cell resolution in pathophysiological conditions utilizing the novel mouse strain and *in vivo* imaging technique with two-photon microscope.[24, 25]

Methods

Animals. GO-ATeam2 mice were generated in our laboratory, which will be described in a separate paper,[23, 26] (manuscript in preparation by M. Yamamoto). They were housed in specific pathogen-free facility and received a routine diet. Ten-fourteen-week-old male mice were used for the *in vivo* imaging. All animal experiments were approved by the Animal Research Committee, Graduate School of Kyoto University, and performed in accordance with the Guide for the Care and Use of Laboratory Animals (NIH).

Mice treatment. Mice were anaesthetized with 2% isoflurane inhalation. The left kidney was exteriorized through a small incision. IR injury was induced by clamping unilateral renal pedicle for each length of time.[27] We analyzed four mice in each group, as previously described in kidney intravital imaging reports.[28, 29] We kept both the core body temperature and the kidney surface temperature 36 °C during warm IR by using two heater systems as described below in *In Vivo two-photon Imaging Settings*. During cold IR experiment, the temperature of core body and the kidney surface were kept 33 °C and 24 °C, respectively. The heart rate was kept more than 450 bpm, and breathing rate was kept more than 100 per minute, by adjusting the dose of anesthesia continuously during imaging studies.

Cell culture and Treatment. Primary tubular cells were isolated and cultured from one-two-week-old GO-ATeam2 mice. The kidneys were minced and digested in 1.25 mg/ml dispase for 30 minutes at 37 °C. After removal of undigested fragments, the digested tissues were washed with PBS, and were suspended in DMEM supplemented with 10 % bovine calf serum, 50 U/ml penicillin, and 50 μg/ml streptomycin. Cells were grown in cell culture dishes for 4 days.

Microscopy and image processing. For two-photon excitation microscopy, we used

FV1200MPE-BX61W1 upright microscope equipped with a 25×/1.05NA water-immersion objective lens (XLPLN25XW-MP; Olympus, Tokyo, Japan) and an Insight DeepSee Ultrafast Laser (Spectra Physics, Mountain View, CA). The excitation wavelength for GFP was 930nm. We used an IR-cut filter, BA750RXD, two dichronic mirrors, DM505 and DM690, and two emission filters, BA495-540 (Olympus) for GFP, and BA562-596 (Olympus) for OFP, respectively. Images were analyzed with MetaMorph software (Universal Imaging, West Chester, PA). Our microscopy allows us to detect tubules within 40 μm from the surface of the kidney in high enough resolution to differentiate between PTs and DTs. We took images at 20 μm from the surface of the kidney to analyze images without the effect of light scattering and absorption.

In Vivo two-photon Imaging Settings. Anaesthetized mice were placed on an electric adjustable heater pad. The kidney was attached to the vacuum-stabilized cup with imaging window,[30] which was also equipped with heater function. Using two heater systems, we controlled both the core body and the kidney temperature during all experimental procedures. The bowl of the imaging window is designed to be filled with water for the water-immersion. Detailed schemes of the vacuum-stabilized imaging window were described in the previous study.[30]

Analysis of ratio changes in tubules. Quantification of ratio was performed using MetaMorph software (Universal Imaging Corporation, Downingtown, PA). The ratio in each tubular section was calculated in the area described in Supplemental Figure 1A. Averages of ratios in five PT sections were utilized as the mean ratios of PTs in the mouse, and the averages from three to four mice were shown in the figures (n = 4 in Figure 1E, 3B and 6B, n = 3 in Figure 2C and Supplemental figure 4C). As for DTs, because the numbers of DT sections in one view are limited, averages of around three DT sections were utilized as the mean ratios of DTs in the mouse, and the averages from four mice were shown in the figures (n = 4 in Figure 1E, 2D, and

3C). The ATP recovery slopes in S1 PTs were calculated as the slope between 0 to 2 minutes after the induction of reperfusion. The ATP % recoveries were calculated in comparisons between the ratios before ischemia and the ratios 60 minutes after the induction of reperfusion.

Renal histochemistry. The harvested kidney samples were fixed in Carnoy's solution, embedded in paraffin, sectioned (2.0μm), and stained periodic acid-Schiff (PAS). All of the PAS samples were analyzed with a Zeiss Axio Imager A2 microscope using Zeiss Axio Vision 4.8 software.

Renal immunofluorescence. The harvested kidney samples were fixed in 4 % paraformaldehyde, incubated in 20 % sucrose in PBS at 4 ℃ overnight and incubated in 30 % sucrose overnight. OCT-embedded kidneys were cryosectioned into 6.0 μm sections. The following primary antibodies were used for immunostaining: anti-αSMA (catalog C 6198; Sigma-Aldrich), and anti-Tim-1/Kim-1 (catalog 14-5861-82; eBioscience).

Quantitative Assessment of fibrosis. Quantification of fibrosis was performed by measuring the α-SMA-positive area in the interstitium, as described previously.[31] Eight images of each kidney section at cortical fields (×200 magnification) were taken in whole circumference with a confocal microscope (n = 4 in each group). All images were obtained using the same laser power and gain intensity with a confocal microscope (FV1000D; Olympus). α-SMA-positive areas in the vascular smooth muscle cells was excluded. The α-SMA-positive areas were automatically calculated by MetaMorph software (Universal Imaging Corporation, Downingtown, PA)

Quantification of mRNA by Real-time PCR. RNA extraction and real-time RT-PCR was performed, as described previously (n = 4 in each group).[31] Specific primers utilized in our previous work[27] were utilized in this study.

Compounds administration. NO-donor (catalog 345-06941; Fuji Film Wako) (3 mg/kg, n = 3) was administered to mice by intravenous injection 5 minutes before IR. 5-Aminoimidazole-4-carboxamide 1-β-D-ribofuranoside (AICAR) (catalog number 011-22533; Fuji Film Wako) (500 mg/kg, n = 3) was administered to mice by intraperitoneal injection for 3 consecutive days and 2 hours before IR. Nicotinamide mononucleotide (NMN) (gifted from Professor Yo-ichi Nabeshima) (500 mg/kg, n = 3) was administered to mice by subcutaneous injection for 6 consecutive days and 3 hours before IR.

Statistics. Results are presented as means ± SD (Figure 2C, 2D, 3B, 3C, 6B, and Supplemental Figure 4C). Some data are reported as box and whisker plots (Figure 4B, 4C, 5B and Supplemental Figure 4B). Statistical significance was assessed by a 2-tailed Student's *t* test for comparisons between two groups (Figure 5B and Supplemental Figure 2A), 1-way ANOVA with Bonferroni's post-hoc tests for comparisons among more than 2 groups (Figure 1E), 1-way ANOVA (Figure 4B, 4C and Supplemental Figure 4B), and the nonparametric test for trend across 15, 30, 60 minute warm IR groups developed by Cuzick, which is an extension of the Wilcoxon rank-sum test (Figure 4B, 4C and 5B). Comparisons between the ATP recovery slopes were assessed by ANCOVA (Figure 3D and 6C). Correlations were determined by Pearson's correlation analysis (Figure 5C, 6D, and 6E). We conducted statistical analyses by Stata (StataCorp®, College Station, TX, USA), version 15.1, with values of $P < 0.05$ considered statistically significant.

Study approval. All animal studies were approved by the Animal Research Committee, Graduate School of Medicine, Kyoto University, and performed in accordance with the National Institute of Health Guide for the Care and Use of Laboratory Animals.

Results

Visualization of ATP levels at a single cell resolution in the kidney with GO-ATeam2 mice

A FRET-based fluorescent ATP probe, termed as GO-ATeam, has been developed for ATP imaging at the single cell resolution,[22, 32] in which variants of green fluorescent protein (GFP) and Kusabira orange fluorescent protein (OFP) sandwich the ε-subunit of *Bacillus subtilis* F_oF_1-ATP synthase (Figure 1A).[32] The ε subunit binds to ATP dose-dependently and specifically, but not to ADP, dATP or GTP.[22] Therefore, the ratio of OFP to GFP emission reflects intracellular ATP levels.[22, 32] The probe is almost insensitive to pH within the physiological ranges.[32]

Recently, we generated a novel mouse line systemically expressing GO-ATeam by inserting *CAG* promoter-driven *GO-ATeam* in *ROSA26* locus (GO-ATeam2 mice).[23, 26] The expression of *GO-ATeam* is ubiquitous, allowing ATP visualization in various tissues. Utilizing this mouse line named GO-ATeam2 mice, we visualized renal ATP of living mice with a two-photon microscope. In the FRET ratio image (Figure 1B, right), warm colors indicate high FRET ratios (high ATP levels) and cool colors indicate low FRET ratios (low ATP levels). There were also tubules with high GO-ATeam expression (Figure 1B, middle). In order to identify the segments of these tubules, we administered 3kDa Texas-red dextran to visualize tubular flow (Figure 1C) as previously reported.[33, 34] The sequences of the flow indicated that these tubules with high intensity signals were DTs. The laser power was reduced to take images of DT without saturation of OFP signal (Figure 1D, right). Among PTs, apical signals in some tubules (*) were relatively higher than others (Figure 1B). According to the sequences of the flow (Figure 1C), PTs with higher apical signals were considered as S1 segments, and PTs with lower apical signals were considered as S2 segments. This result is in accordance with the previous study demonstrating high autofluorescence in apical sides of S1 segments of wild-type mice.[35] Because of the high autofluorescence, apical sides of S1 segments of proximal tubules were excluded during monitoring FRET ratios (Supplemental Figure 1A). S3 segments of PTs were

not observed from the surface of the kidney.

While the ATP levels in PTs were homogeneous (Figure 1D, left), the ATP levels of DTs and collecting ducts were heterogeneous (Figure 1D, right). As for the evaluation of the ratios in DTs, we averaged the results of all cells in each DT section, whereas we selected principal cells in the evaluation of CDs, because we could not obtain required signal in intercalated cells (Supplemental Figure 1A). Immunostaining revealed higher expression of GO-ATeam in principal cells, and lower expression in intercalated cells (Supplemental Figure 1B). We assume that the different expression of biosensor between two cell types is due to the characteristics of CAG promoter driving FRET probe.

The FRET ratios in S1 and S2 segment of PTs, DTs and collecting ducts (principle cells) were higher in DTs and collecting ducts than in PTs (Figure 1E).

Rapid ATP reduction in PTs and slow ATP reduction in DTs after ischemia

In addition to the heterogeneity in basal ATP concentrations between cell types in kidney, we expected that ATP dynamics upon AKI would vary between cell types because of the different ATP demands and energy metabolism. We first confirmed that renal dysfunction as well as histological injury of GO-ATeam2 mice were comparable with those of wild-type mice after ischemic reperfusion (IR) injury (Supplemental Figure 2).

To analyze spatiotemporal ATP dynamics during AKI, we next performed ATP imaging on the kidneys of GO-ATeam2 mice upon induction of IR injury. S1, S2 PTs and DTs were identified by the autofluorescence features and FRET patterns described in the previous section.

As expected, we noticed the crucial difference of ATP dynamics between PTs and DTs during ischemia (Figure 2, Supplemental Movie A). While the ATP levels in both S1 and S2 segments of PTs decreased rapidly and homogenously, and reached the minimum plateau within two minutes after the induction of ischemia (Figure 2, A and C), the ATP levels in DTs and CDs decreased very slowly, reaching the minimum plateau after 60 minutes (Figure 2, B and D).

ATP reduction rates were heterogeneous even within DTs and CDs (Figure 2, A and B, Supplemental movie A). In contrast, the ATP levels in interstitial cells were well maintained (Figure 2E).

ATP recovery in PTs after reperfusion varies depending on the length of ischemia

Next, we analyzed the recovery of ATP after IR in GO-Ateam2 mice. We induced 15, 30, and 60 minute-warm ischemia and monitored ATP dynamics in each segment after reperfusion (Supplemental Movie B). While the minimum plateau ATP levels in PTs after warm 15, 30, and 60 minute-ischemia were similar, longer ischemia resulted in slower recovery of ATP in PTs (Figure 3A). The ATP recovery in S1 PTs during reperfusion after warm 15, 30, and 60 minute-ischemia took 2, 5, and 30 minutes to reach a peak plateau, and the % ATP recovery were 92.3 ± 4.1%, 86.2 ± 3.8%, and 69.6 ± 4.1%, respectively (Figure 3B). The ATP recovery slopes in S1 PTs between 0 to 2 minutes after 15, 30, and 60 minute-ischemia reperfusion were 0.446 ± 0.016, 0.277 ± 0.052, and 0.075 ± 0.064, respectively, showing by analysis of covariance (ANCOVA) that longer ischemia resulted in lower recovery slopes (Figure 3D). The % ATP recoveries in S2 PTs after warm 15, 30, and 60 minute-ischemia was 92.6 ± 3.6%, 84.0 ± 10.9%, and 25.5 ± 10.6%, indicating that S2 PTs were more vulnerable than S1 PTs in the severe IR injury (Figure 3B). In addition, significant vacuolization was observed in S2 PTs, but not in S1 PTs (Supplemental Figure 3).

ATP recovery in DTs is rapid and almost complete, even after long ischemia

The ATP dynamics in DTs was strikingly different from those of PTs. First, the ATP level continued to decrease until 60 min (Figure 2D). Second, the ATP levels in DTs recovered quickly and almost completely even after 60-minute-ischemia (Figure 3, A and C). ATP recovery in DTs after warm 15, 30, and 60-minute ischemia only took 1, 2, and 4 minutes to reach a peak plateau, and the % ATP recoveries were 87.5± 7.4%, 89.8 ± 7.0%, and 89.2 ±

5.0 %, respectively, indicating the resistance of DTs to IR injury (Figure 3C).

Mitochondrial damage and PTC flow after reperfusion might be the determinants of ATP recovery

To explore the determinants of the ATP recovery after reperfusion, we next examined mitochondrial injury 5 minutes after reperfusion. Mitochondrial fragmentation was obvious in PTs after reperfusion (Figure 4A), and by the nonparametric trend test,[36] the longer ischemic time resulted in the increase of fragmented mitochondria in PTs (Figure 4B). On the contrary, no obvious mitochondrial fragmentation was observed in DTs even after long ischemia (Figure 4A). We also visualized peritubular capillary (PTC) flow five minutes after reperfusion utilizing two-photon microscopy[37] (Supplemental Movie C1), and found that the longer ischemia time resulted in decreased PTC flow by the nonparametric trend test (Figure 4C). Red blood cell rouleaux formation leading to the instability of PTC flow was also confirmed after 60 minute-ischemia (Supplemental Movie C2). Statistical differences between groups in Figure 4B and 4C were also confirmed by ANOVA.

Fibrosis in chronic phase is inversely correlated with the ATP recovery in acute phase

Fibrosis in chronic phase after AKI is often regarded as the sign of poor renal prognosis.[38] Histological analysis of fibrosis, measurement of αSMA-positive area, and realtime RT-PCR of *αSMA* mRNA on day 14 after IR revealed the progression of renal fibrosis after longer warm ischemia by the nonparametric test for trend (Figure 5, A and B). We next analyzed the correlation between the ATP recovery slopes in acute phase and αSMA positive area in chronic phase by Pearson's correlation analysis, and surprisingly, found that αSMA positive area in chronic phase was inversely well correlated with the ATP recovery of PTs in acute phase (Figure 5C), indicating that the ATP recovery of PTs in acute phase is an important predictor of renal prognosis.

Renal hypothermia improves ATP recovery in acute phase and fibrosis in chronic phase after IR injury

Renal hypothermia may decrease the metabolic demand of nephrons, and is expected to protect the kidney from IR injury.[39, 40] The efficacy of renal hypothermia has been tested in clinical practice of kidney transplantation from diseased donors[41] and partial nephrectomy.[42] However, the mechanism of its protective effects remained unclear. We hypothesized that hypothermia protects kidney from ischemia by suppressing depletion of ATP.

We examined the effect of hypothermia on ATP dynamics during IR by holding the core body temperature at 33 °C. The ATP recovery after 30 and 60 minute-ischemia was dramatically improved in cold ischemia group (Figure 6A). The ATP recovery in S1 PTs after cold 30 and 60 minute-ischemia took only 2 and 4 minutes to reach a peak plateau (Figure 6B), while the ATP recovery after warm 30 and 60 minute-ischemia took 5 and 30 minutes (Figure 3B). The % ATP recovery after cold 30 and 60 minute-ischemia was 90.6 ± 2.5 % and 87.1 ± 2.6 % (Figure 6B) while those after warm 30 and 60 minute-ischemia was 86.2 ± 3.8 % and 69.6 ± 4.1 % (Figure 3B). The ATP recovery slopes in S1 PTs after cold 30 and 60 minute-ischemia were 0.496 ± 0.037 and 0.326 ± 0.049 (Figure 6C), while those after warm 30 and 60 minute-ischemia were 0.277 ± 0.052 and 0.075 ± 0.064 (Figure 3D).

To exclude the possibility that temperature affected the properties of GO-ATeam2, we analyzed the ratios in primary cells obtained from the kidneys of GO-ATeam2 mice sequentially cultured under different temperatures, and found similar ratios by ANOVA (P = 0.86) (Supplemental Figure 4, A and B). We also confirmed that the body temperature changes did not affect the ratios by monitoring ratios of mice treated with cold 30 and 60 minute-IR, whose kidney were warmed 50 minutes after reperfusion (Supplemental Figure 4C). Thus, we concluded that the temperature itself did not affect the FRET ratio in our experimental setup.

Additionally, cold IR remarkably ameliorated renal fibrosis in chronic phase (Figure 5, A and

B). Inverse correlation between the ATP recovery slope in acute phase and αSMA positive area in chronic phase was well maintained even when we evaluated kidney samples treated with warm and cold ischemia together (Figure 6D). The fibrosis area was also inversely correlated with % ATP recovery in acute phase (Figure 6E).

Discussion

The conventional ATP quantification methods, such as luciferase assay, nuclear magnetic resonance spectroscopy, and mass imaging technique have not allowed us to visualize and monitor spatiotemporal ATP dynamics *in vivo*. Here we have successfully visualized ATP levels at a single cell resolution in the living kidney, and demonstrated spatiotemporal ATP dynamics during IR injury for the first time.

First we showed that, in the physiological condition, the cytoplasmic ATP levels in S1 PTs were higher than those in S2, and were lower than those in DTs, in accordance with the previous reports analyzing ATP in dissected nephron by the luciferin-luciferase technique.[16, 43, 44] Lower basal ATP levels in S2 PT, even though this is regarded as a metabolically active region, might suggest higher consumption of ATP in this segment.

We also revealed the cell-type specific ATP dynamics during IR injury and demonstrated that the ATP levels in PTs decreased rapidly upon ischemia induction, whereas the ATP levels in DTs decreased very slowly. Our results are in accordance with the histological resistance of DTs to IR injury compared to PTs.[21] There are several possible explanations for different ATP dynamics during IR injury. First, under ischemia, DTs could produce ATP by anaerobic glycolysis while PTs depend mainly on aerobic ATP production for energy supply.[17, 18] Second, mitochondrial function might be also different between segments. Previous study demonstrated that mitochondrial membrane potential was better maintained after the inhibition of respiration in DTs than in PTs.[28, 45] Our data showing more fragmentation of mitochondria in PTs compared to that in DTs after IR injury (Figure 4A) also supports the hypothesis. Third, higher expression of cytoprotective factors such as Bcl-2 and heat shock proteins in DTs might also contribute to the resistance.[46] Fourth, the energy consumption of PTs might be higher than that of DTs, which leads to the rapid ATP fall in PTs after ischemia.

Next, we showed that the ATP recovery in PTs after IR was dependent on the severity of injury (Figure 3). There are several possible mechanisms explaining slow and insufficient ATP

recovery after longer ischemia, such as mitochondrial dysfunction (Figure 4, A and B) and oxygen supply reduction due to microvascular rarefaction, decreased peritubular capillary (PTC) flow (Figure 4C), and coagulation.

We also showed slower and insufficient ATP recovery and more vacuolization in S2 PTs than in S1 PTs, indicating that S2 PTs are more susceptible to ischemia than S1 PTs. A previous study demonstrated the resistant of S1 PTs to oxidative stress in sepsis model, possibly by the upregulation of cytoprotective heme oxygenase-1 and sirtuin-1.[29] The decrease of tubular flow and accumulation of debris could also contribute to higher susceptibility of S2 PTs.

One hour after the induction of reperfusion, neither obvious histological injury nor the expression of Kim-1 was observed even in the kidneys treated with warm 60 minute-ischemia, indicating the dynamic changes of cytoplasmic ATP could occur before obvious histological injury (Supplemental Figure 5A). One day after IR, the kidneys treated with warm ischemia showed cell detachment of tubule epithelial cells (Supplemental Figure 5, A and B), while cold IR dramatically ameliorated tubular injury. These differences in histological findings in acute phase are consistent with the different ATP dynamics in each group.

More importantly, we revealed that the fibrosis area in chronic phase was inversely correlated with the ATP recovery slope and % ATP recovery in PTs in acute phase. These results strongly indicate that breakdown of ATP homeostasis in PTs plays an important role in AKI to CKD progression, and that the initial ATP recovery of PTs could be the primary determinant of the renal prognosis in ischemic AKI.

Finally, we provide the direct *in vivo* evidence that hypothermia during IR injury improves the ATP recovery as well as fibrosis (Figure 5, 6). Previous studies showed that renal hypothermia conferred striking protection against IR injury[39, 40, 47], possibly by decreasing the renal oxygen demand and metabolic activity. Our study provided direct evidence supporting previous hypothesis. We further succeeded in the quantitative comparison of ATP dynamics during warm and cold IR with respect to the speed and extent of the ATP recovery. Our results demonstrated

the ATP dynamics of cold 30 minute-ischemia in S1 PTs was slightly better than that of warm 15 minute-ischemia, and the ATP recovery of cold 60 minute-ischemia was better than that of warm 30 minute-ischemia (Figure 3 and 6). These results suggest that in cold conditions, similar ATP dynamics are obtained even with ischemic time about twice longer than that of warm conditions in mice. Human kidneys are exposed to ischemia in the surgical procedures of transplantation and partial nephrectomy, and renal hypothermia is often applied in the clinical settings. Some clinical studies assessed renal function after partial nephrectomy[48-51] and concluded that longer warm ischemia time is associated with poor renal prognosis. One report analyzing renal function after warm and cold ischemia during partial nephrectomy utilizing ^{99m}Tc-mercaptoacetyltriglycine renal scintigraphy parameters revealed that the cold condition enabled to extend ischemia time more than twice of warm condition in humans.[49] There is also the accumulating evidence for metabolic dysfunction during ischemic AKI in human renal transplantation.[52] These finding are not only in accordance with our study showing the significance of the association between ATP dynamics and prognosis, but also implies that our ATP visualization technique has the potential to elucidate cellular mechanism of AKI to CKD progression.

Recently, new potential approaches focusing on the attenuation of endothelial dysfunction (NO-donor)[53], AMPK activator (AICAR)[54], mitochondrial biogenesis and cellular bioenergetics, such as MitoQ, skQR1, SS-31, MA-5, peroxisome proliferator, and NMN[10, 55-59] have been developed and some of them showed renoprotective effect. We examined whether the administration of NO-donor, AICAR, and NMN could improve the ATP dynamics in acute phase, but failed to show the improvement of the ratio before IR, the recovery slope, or the % recovery (Supplemental Figure 6, A and B). Discrepancy with previous reports might be explained by the difference in the protocols.

Although intravital imaging of kidney of GO-ATeam2 mice provides invaluable information on the ATP dynamics of the kidney, there remain several technical limitations to be challenged in

the future: (1) We could not reach deeper kidney regions such as PT S3 segments and interstitial cells in corticomedullary junction by two-photon microscopes. The ATP dynamics of deeper cortical regions after IR injury might be more intense than that of the kidney surface. While the ATP levels of interstitial cells in the kidney surface were maintained after IR injury (Figure 2E), it is likely that interstitial cells in deeper kidney regions would show diminished ATP levels after IR injury, consistent with their well-established oxygen sensing function and erythropoietin synthesis. Development of another FRET probe that operates at longer wavelength may alleviate the light scattering, and thereby enables deep tissue imaging. (2) The cellular ATP levels visualized in our mice are the results of a balance between production and consumption; therefore, rate of ATP production or consumption cannot be assessed separately. Even with these limitations, the analysis utilizing the novel ATP imaging technique shed light on tubular ATP dynamics *in vivo* during AKI, and revealed the crucial difference of the ATP dynamics between nephron segments, and more importantly, highlighted the correlation between ATP recovery of PTs in acute phase and renal prognosis. This revolutionary ATP imaging technique improves our understanding of the cellular events in the diseased kidney and could help us to develop therapeutic strategies to treat AKI and to minimize IR injury following kidney transplantation and partial nephrectomy.

22

1
2
3
4
5
6
7
8
9
10
11
12
13
14
15
16
17
18
19
20
21
22
23
24
25
26
27
28
29
30
31
32
33
34
35
36
37
38
39
40
41
42
43
44
45
46
47
48
49
50
51
52
53
54
55
56
57
58
59
60

Author contributions

ShinY and MoY designed the experiments and wrote the manuscript. MoY supervised the project. ShinY, MaY, JN, AM, ShigeY, MT, KK, YS performed experiments and ShinY, MaY, EU, SF, HI and MM analyzed the data.

Acknowledgment

Authors would like to thank Dr. Minoru Satoh and Dr. Daisuke Nakano for valuable discussion regarding the live imaging, and Ms. Satsuki Fujiwara and Ms. Kanako Takakura for technical assistance, and Dr. Keita Hirano for statistical analysis, and Dr. Kousuke Nakata for figure illustration, and Professor Yo-ichi Nabeshima for gifted NMN. This work was supported by Platform for Drug Discovery, Informatics, and Structural Life Science from the Ministry of Education, Culture, Sports, Science and Technology, Japan and by Kyoto University Live Imaging Center and in part by Grants-in-Aid KAKENHI 16H06280 "ABiS". This research was partially supported by the Japan Agency for Medical Research and Development (AMED) under Grant Number JP19gm5010002, JP19gm0610011 and AMED-CREST19gm1210009 to MoY; partially by grants from the TMK Project, KAKENHI Grant-in-Aids for Scientific Research B (17H04187, 20H03697), Grant in Aid for Scientific Research on Innovative Areas "Stem Cell Aging and Disease (17H05642)" and "Lipoquality (18H04673)" from Ministry of Education, Culture, Sports, Science and Technology of Japan, grants from the Uehara Memorial Foundation, Takeda Science Foundation, and the Sumitomo Foundation. This work was partly supported by World Premier International Research Center Initiative (WPI), MEXT, Japan. This study was also partly supported by JST PRESTO under Grant Number JPMJPR14MF to MaY.

Disclosure

YS is employed by TMK project. MY receives research grants from Astellas, Chugai, Daiichi Sankyo, Fujiyakuhin, Kyowa Hakko Kirin, Mitsubishi Tanabe, MSD, Nippon Boehringer Ingelheim, and Torii. Other authors report no conflicts of interest.

Supplementary material table of contents

References

1. Lewington AJ, Cerda J, and Mehta RL: Raising awareness of acute kidney injury: a global perspective of a silent killer. *Kidney Int* 84: 457-467, 2013.
2. Chertow GM, Burdick E, Honour M, Bonventre JV, and Bates DW: Acute kidney injury, mortality, length of stay, and costs in hospitalized patients. *J Am Soc Nephrol* 16: 3365-3370, 2005.
3. Coca SG, Singanamala S, and Parikh CR: Chronic kidney disease after acute kidney injury: a systematic review and meta-analysis. *Kidney Int* 81: 442-448, 2012.
4. Ishani A, Xue, JL, Himmelfarb, J, Eggers, PW, Kimmel, PL, Molitoris, BA, et al.: Acute kidney injury increases risk of ESRD among elderly. *J Am Soc Nephrol* 20: 223-228, 2009.
5. Sato, Y, Takahashi, M, Yanagita, M: Pathophysiology of AKI to CKD progression. *Semin Nephrol* 40: 206-215, 2020.
6. Lan R, Geng H, Singha PK, Saikumar P, Bottinger EP, Weinberg JM, et al.: Mitochondrial Pathology and Glycolytic Shift during Proximal Tubule Atrophy after Ischemic AKI. *J Am Soc Nephrol* 27: 3356-3367, 2016.
7. Kang, HM, Ahn, SH, Choi, P, Ko, YA, Han, SH, Chinga, F, et al.: Defective fatty acid oxidation in renal tubular epithelial cells has a key role in kidney fibrosis development. *Nat Med* 21: 37-46, 2015.
8. Tran, MT, Zsengeller, ZK, Berg, AH, Khankin, EV, Bhasin, MK, Kim, W, et al.: PGC1alpha drives NAD biosynthesis linking oxidative metabolism to renal protection. *Nature* 531: 528-532, 2016.
9. Szeto HH: Pharmacologic Approaches to Improve Mitochondrial Function in AKI and CKD. *J Am Soc Nephrol* 28: 2856-2865, 2017.
10. Poyan Mehr A, Tran, MT, Ralto, KM, Leaf, DE, Washco, V, Messmer, J, et al.: De

novo NAD(+) biosynthetic impairment in acute kidney injury in humans. *Nature Med* 24: 1351-1359, 2018.

11. Knowles JR: Enzyme-catalyzed phosphoryl transfer reactions. *Annu Rev Biochem* 49: 877-919, 1980.
12. Siegel NJ, Devarajan P, and Van Why S: Renal cell injury: metabolic and structural alterations. *Pediatr Res* 36: 129-136, 1994.
13. Avison MJ, van Waarde A, Stromski ME, Gaudio K, and Siegel NJ: Metabolic alterations in the kidney during ischemic acute renal failure. *Semin Nephrol* 9: 98-101, 1989.
14. Stromski ME, Cooper K, Thulin G, Gaudio KM, Siegel NJ, and Shulman RG: Chemical and functional correlates of postischemic renal ATP levels. *Proc Natl Acad Sci U S A* 83: 6142-6145, 1986.
15. Vogt MT, and Farber E: On the molecular pathology of ischemic renal cell death. Reversible and irreversible cellular and mitochondrial metabolic alterations. *Am J Pathol* 53: 1-26, 1968.
16. Uchida S, and Endou H: Substrate specificity to maintain cellular ATP along the mouse nephron. *Am J Physiol* 255: F977-983, 1988.
17. Wirthensohn G, and Guder WG: Renal substrate metabolism. *Physiol Rev* 66: 469-497, 1986.
18. Bagnasco S, Good D, Balaban R, and Burg M: Lactate production in isolated segments of the rat nephron. *Am J Physiol* 248: F522-526, 1985.
19. Vandewalle A, Wirthensohn G, Heidrich HG, and Guder WG: Distribution of hexokinase and phosphoenolpyruvate carboxykinase along the rabbit nephron. *Am J Physiol* 240: F492-500, 1981.
20. Sharfuddin AA, and Molitoris BA: Pathophysiology of ischemic acute kidney injury. *Nat Rev Nephrol* 7: 189-200, 2011.

21. Lieberthal W, and Nigam SK: Acute renal failure. I. Relative importance of proximal vs. distal tubular injury. *Am J Physiol* 275: F623-31, 1998.

22. Imamura H, Nhat, KP, Togawa, H, Saito, K, Iino, R, Kato-Yamada, et al.: Visualization of ATP levels inside single living cells with fluorescence resonance energy transfer-based genetically encoded indicators. *Proc Natl Acad Sci U S A* 106: 15651-15656, 2009.

23. Yamamoto M, Kim M, Imai H, Itakura Y, and Ohtsuki G: Microglia-Triggered Plasticity of Intrinsic Excitability Modulates Psychomotor Behaviors in Acute Cerebellar Inflammation. *Cell Rep* 28: 2923-2938.e8, 2019.

24. Ashworth SL, Sandoval RM, Tanner GA, and Molitoris BA: Two-photon microscopy: visualization of kidney dynamics. *Kidney Int* 72: 416-421, 2007.

25. Peti-Peterdi J, Kidokoro K, and Riquier-Brison A: Novel *in vivo* techniques to visualize kidney anatomy and function. *Kidney Int* 88: 44-51, 2015.

26. Nakano, M, Imamura, H, Sasaoka, N, Yamamoto, M, Uemura, N, Shudo, T, et al.: ATP Maintenance via Two Types of ATP Regulators Mitigates Pathological Phenotypes in Mouse Models of Parkinson's Disease. *EBioMedicine* 22: 225-241, 2017.

27. Endo, T, Nakamura, J, Sato, Y, Asada, M, Yamada, R, Takase, et al.: Exploring the origin and limitations of kidney regeneration. *J Pathol* 236: 251-263, 2015.

28. Hall AM, Rhodes GJ, Sandoval RM, Corridon PR, and Molitoris BA: *In vivo* multiphoton imaging of mitochondrial structure and function during acute kidney injury. *Kidney Int* 83: 72-83, 2013.

29. Kalakeche, R, Hato, T, Rhodes, G, Dunn, KW, El-Achkar, TM, Plotkin, Z, et al.: Endotoxin uptake by S1 proximal tubular segment causes oxidative stress in the downstream S2 segment. *J Am Soc Nephrol* 22: 1505-1516, 2011.

30. Sano, T, Kobayashi, T, Negoro, H, Sengiku, A, Hiratsuka, T, Kamioka, Y, et al.:

Intravital imaging of mouse urothelium reveals activation of extracellular signal-regulated kinase by stretch-induced intravesical release of ATP. *Physiol Rep* 4, 2016.

31. Takaori, K, Nakamura, J, Yamamoto, S, Nakata, H, Sato, Y, Takase, M, et al.: Severity and Frequency of Proximal Tubule Injury Determines Renal Prognosis. *J Am Soc Nephrol.* 27: 2393-2406, 2016.

32. Nakano M, Imamura H, Nagai T, and Noji H: Ca(2)(+) regulation of mitochondrial ATP synthesis visualized at the single cell level. *ACS Chem Biol* 6: 709-715, 2011.

33. Molitoris BA, and Sandoval RM: Intravital multiphoton microscopy of dynamic renal processes. *Am J Physiol Renal Physiol* 288: F1084-9, 2005.

34. Nakano, D, Doi, K, Kitamura, H, Kuwabara, T, Mori, K, Mukoyama, M, et al.: Reduction of Tubular Flow Rate as a Mechanism of Oliguria in the Early Phase of Endotoxemia Revealed by Intravital Imaging. *J Am Soc Nephrol* 26: 3035-3044, 2015.

35. Hato, T, Winfree, S, Day, R, Sandoval, RM, Molitoris, BA, Yoder, MC, et al.: Two-Photon Intravital Fluorescence Lifetime Imaging of the Kidney Reveals Cell-Type Specific Metabolic Signatures. *J Am Soc Nephrol* 28: 2420-2430, 2017.

36. Cuzick J: A Wilcoxon-type test for trend. *Stat Med* 4: 87-90, 1985.

37. Kang JJ, Toma I, Sipos A, McCulloch F, and Peti-Peterdi J: Quantitative imaging of basic functions in renal (patho)physiology. *Am J Physiol Renal Physiol* 291: F495-502, 2006.

38. He, L, Wei, Q, Liu, J, Yi, M, Liu, Y, Liu, H, et al.: AKI on CKD: heightened injury, suppressed repair, and the underlying mechanisms. *Kidney Int* 92: 1071-1083, 2017.

39. Ward JP: Determination of the Optimum temperature for regional renal hypothermia during temporary renal ischaemia. *Br J Urol* 47: 17-24, 1975.

40. Zager RA, and Altschuld R: Body temperature: an important determinant of severity of ischemic renal injury. *Am J Physiol* 251: F87-93, 1986.

41. Niemann, CU, Feiner, J, Swain, S, Bunting, S, Friedman, M, Crutchfield, M, et al.: Therapeutic Hypothermia in Deceased Organ Donors and Kidney-Graft Function. *N Engl J Med* 373: 405-414, 2015.

42. Breau, RH, Cagiannos, I, Knoll, G, Morash, C, Cnossen, S, Lavallee, LT, et al.: Renal hypothermia during partial nephrectomy for patients with renal tumours: a randomised controlled clinical trial protocol. *BMJ open* 9: e025662, 2019.

43. Burch, HB, Choi, S, Dence, CN, Alvey, TR, Cole, BR, Lowry, OH, et al.: Metabolic effects of large fructose loads in different parts of the rat nephron. *J Biol Chem* 255: 8239-8244, 1980.

44. Soltoff SP: ATP and the regulation of renal cell function. *Annu Rev Physiol* 48: 9-31, 1986.

45. Hall AM, Unwin RJ, Parker N, and Duchen MR: Multiphoton imaging reveals differences in mitochondrial function between nephron segments. *J Am Soc Nephrol* 20: 1293-1302, 2009.

46. Gobe, GC, Johnson, DW: Distal tubular epithelial cells of the kidney: Potential support for proximal tubular cell survival after renal injury. Int J Biochem cell Biol 39: 1551-1561, 2007.

47. Zager RA, Gmur DJ, Bredl CR, and Eng MJ: Degree and time sequence of hypothermic protection against experimental ischemic acute renal failure. *Circ Res.* 65: 1263-1269, 1989.

48. Thompson, RH, Lane, BR, Lohse, CM, Leibovich, BC, Fergany, A, Frank, I, et al.: Every minute counts when the renal hilum is clamped during partial nephrectomy. *Eur Urol* 58: 340-345, 2010.

49. Funahashi Y, Yoshino Y, Sassa N, Matsukawa Y, Takai S, and Gotoh M: Comparison of warm and cold ischemia on renal function after partial nephrectomy. *Urology* 84: 1408-1412, 2014

50. Volpe, A, Blute, ML, Ficarra, V, Gill, IS, Kutikov, A, Porpiglia, F, et al.: Renal Ischemia and Function After Partial Nephrectomy: A Collaborative Review of the Literature. *Eur Urol* 68: 61-74, 2015.

51. Simmons MN, Lieser GC, Fergany AF, Kaouk J, and Campbell SC: Association between warm ischemia time and renal parenchymal atrophy after partial nephrectomy. *J Urol* 189: 1638-1642, 2013.

52. Wijermars, LG, Schaapherder, AF, de Vries, DK, Verschuren, L, Wust, RC, Kostidis, S, et al.: Defective postreperfusion metabolic recovery directly associates with incident delayed graft function. *Kidney Int* 90: 181-191, 2016.

53. Kurata, H, Takaoka, M, Kubo, Y, Katayama, T, Tsutsui, H, Takayama, J, et al.: Protective effect of nitric oxide on ischemia/reperfusion-induced renal injury and endothelin-1 overproduction. *Eur J Pharmacol*: 517: 232-239, 2005.

54. Lempiäinen, J, Finckenberg, P, Levijoki, J, Mervaala, E: AMPK activator AICAR ameliorates ischaemia reperfusion injury in the rat kidney. *Br J Pharmacol*: 166: 1905-1915, 2012.

55. Dare AJ, Bolton EA, Pettigrew GJ, Bradley JA, Saeb-Parsy K, and Murphy MP: Protection against renal ischemia-reperfusion injury *in vivo* by the mitochondria targeted antioxidant MitoQ. *Redox Biol.* 5: 163-168, 2015.

56. Plotnikov, EY, Chupyrkina, AA, Jankauskas, SS, Pevzner, IB, Silachev, DN, Skulachev, VP, et al.: Mechanisms of nephroprotective effect of mitochondria-targeted antioxidants under rhabdomyolysis and ischemia/reperfusion. *Biochim Biophysi Acta* 1812: 77-86, 2011.

57. Suzuki, T, Yamaguchi, H, Kikusato, M, Hashizume, O, Nagatoishi, S, Matsuo, A, et al.: Mitochonic Acid 5 Binds Mitochondria and Ameliorates Renal Tubular and Cardiac Myocyte Damage. *J Am Soc Nephrol* 27: 1925-1932, 2016.

58. Yang HC, Deleuze S, Zuo Y, Potthoff SA, Ma LJ, and Fogo AB: The PPARgamma

agonist pioglitazone ameliorates aging-related progressive renal injury. *J Am Soc Nephrol* 20: 2380-2388, 2009.

59. Wills, LP, Trager, RE, Beeson, GC, Lindsey, CC, Peterson, YK, Beeson, CC, et al.: The beta2-adrenoceptor agonist formoterol stimulates mitochondrial biogenesis. *J Pharmacol Exp Ther*. 342: 106-118, 2012.

Figure 1

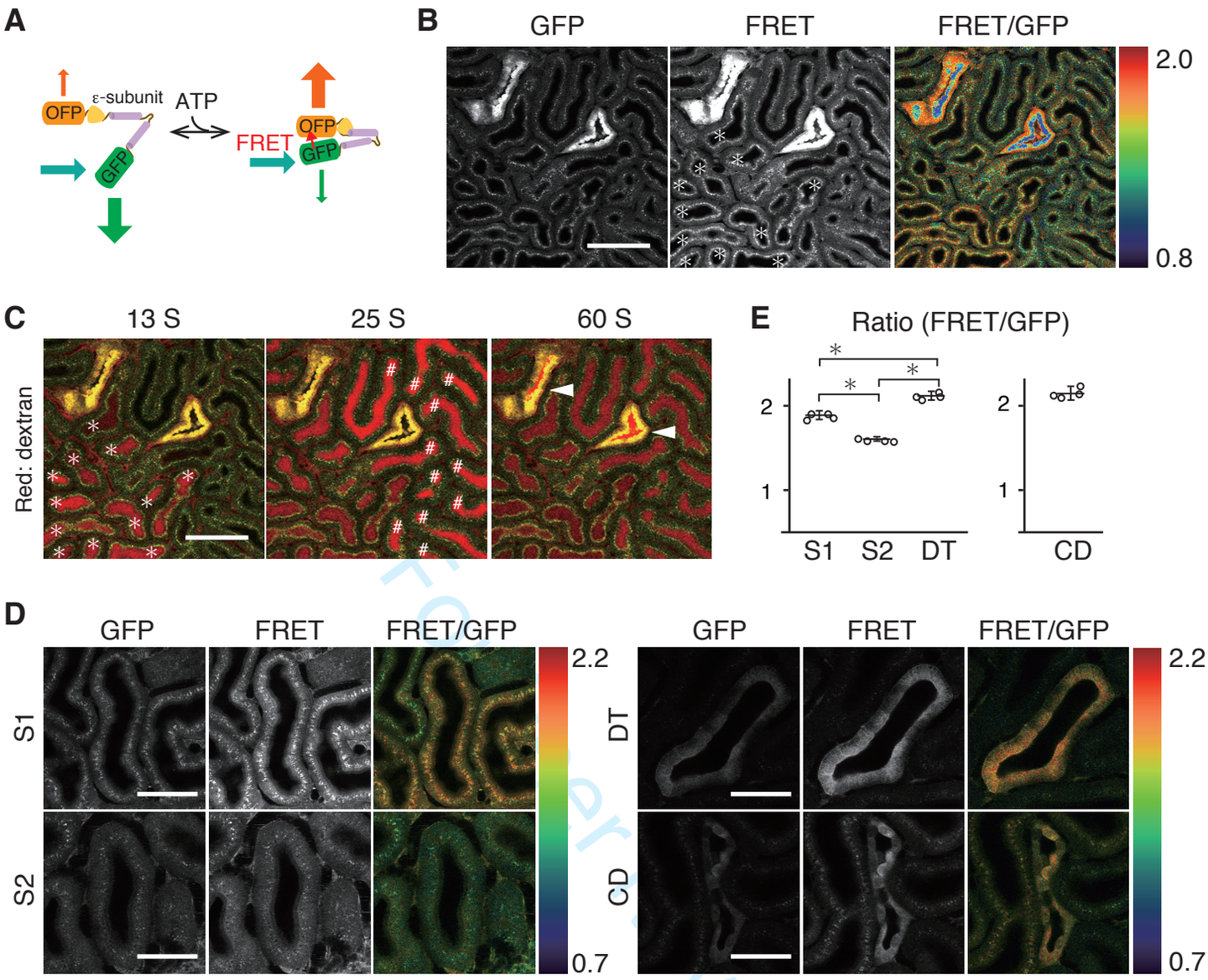

Figure 1. Visualization of ATP levels in the kidney with GO-ATeam2 mice revealed ATP distribution. (**A**) Schematic drawing of a FRET-based fluorescent ATP probe, termed as GO-Ateam. Green fluorescent protein (GFP) and Kusabira orange fluorescent protein (OFP) sandwich the ε subunit of *Bacillus subtilis* FoF1-ATP synthase. (**B**) Images of GFP and FRET signal, and the emission ratio image of FRET to GFP emission. Warm colors indicate high FRET ratios (high ATP levels) and cool colors indicate low FRET ratios (low ATP levels). (**C**) Identification of S1 (*), S2 (#) proximal tubules (PTs) and distal tubules (DTs). In order to identify the segment of these tubules, we administered 3kDa Texas-red dextran to visualize tubular flow. According to the sequences of the flow, PTs with higher apical signals (*) were considered as S1 segments, PTs with lower apical signals were considered as S2 segments (#), and the tubules with high intensity signals were DTs (arrowhead). Note that the ATP levels are not correlated with the signal intensity but with the ratio of FRET to GFP emission. (**D**) Visualization of ATP levels in each segment. While the ATP levels in PTs were homogeneous, the ATP levels of DTs and collecting ducts were heterogeneous. (**E**) Ratios in PT S1, PT S2, DTs, and principal cell in collecting ducts (CDs) (n = 4 mice per group). We presented graphs of CDs separately from those of PTs and DTs, because the ratios in PTs and DTs are the average in each segment and the ratio of CDs is the average in principal cells. Statistical significance among S1 PTs, S2 PTs, and DTs was assessed by 1-way ANOVA with Bonferroni's post-hoc tests for comparisons. $^{*}P < 0.01$.
Scale bars: (**B** and **C**) 100 μm. (**D**) 50 μm.

Figure 2

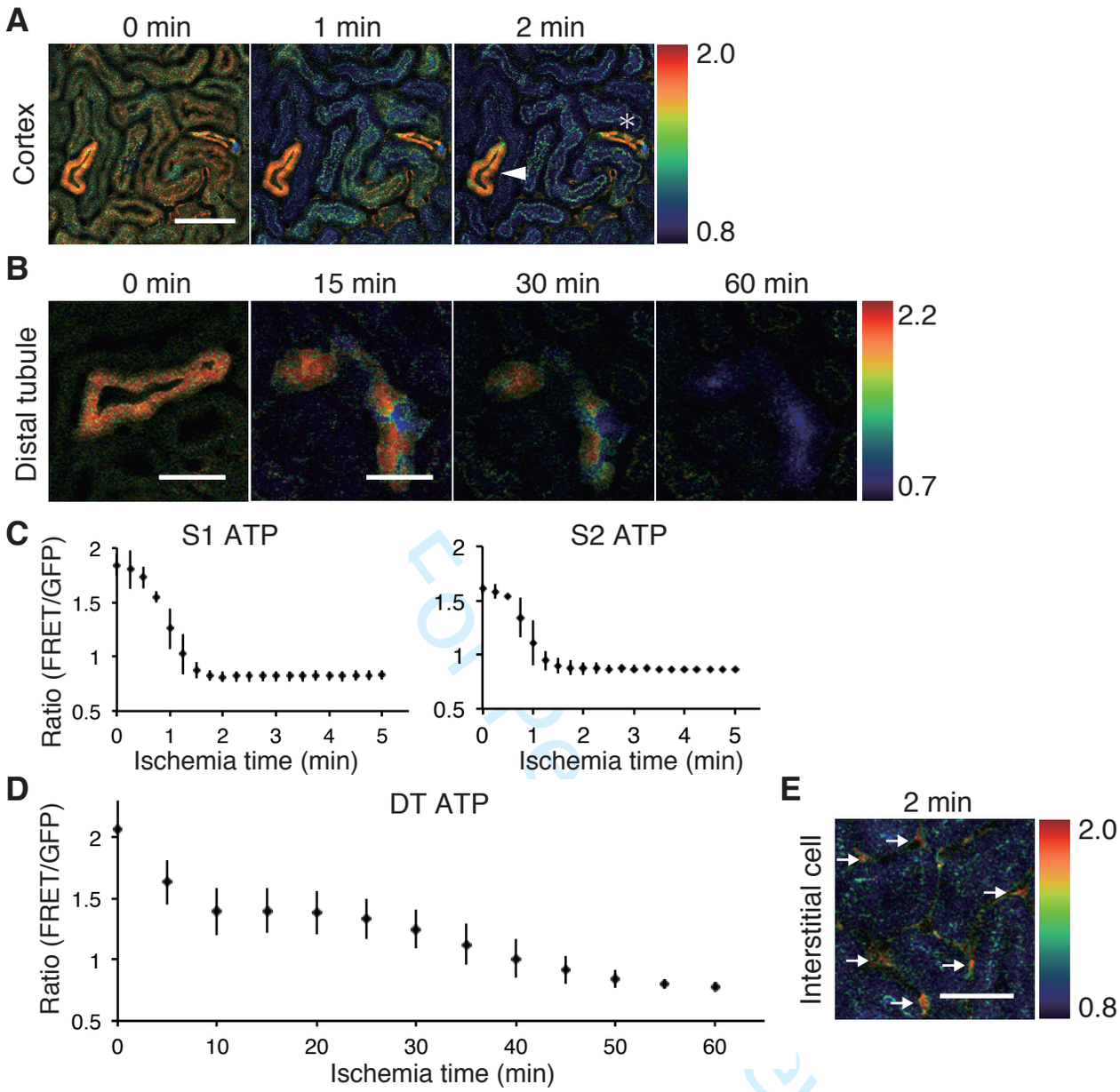

Figure 2. Rapid ATP reduction in PTs and slow ATP reduction in DTs after ischemia. (**A**) Ratio images of PTs, DT, and CD during ischemia. While the ATP levels of PTs decreased very rapidly, in contrast, the ATP levels in DT (arrowhead) and CD (asterisk) were maintained well. (**B**) Ratio images of DT during ischemia. (**C** and **D**) Ratio graphs of S1, S2 PTs and DTs during ischemia. The ATP levels in both S1 and S2 PTs reached the minimum plateau in two minutes (C: n = 3 mice per group) while the ATP levels in DTs were maintained even 30 minutes after induction of ischemia and decreased gradually up to 1 hour (D: n = 4 mice per group). (**E**) The ATP levels in interstitial cells (arrow) were well maintained. Scale bars: (**A** and **E**) 100 µm. (**B**) 50 µm.

35 **Figure 3**

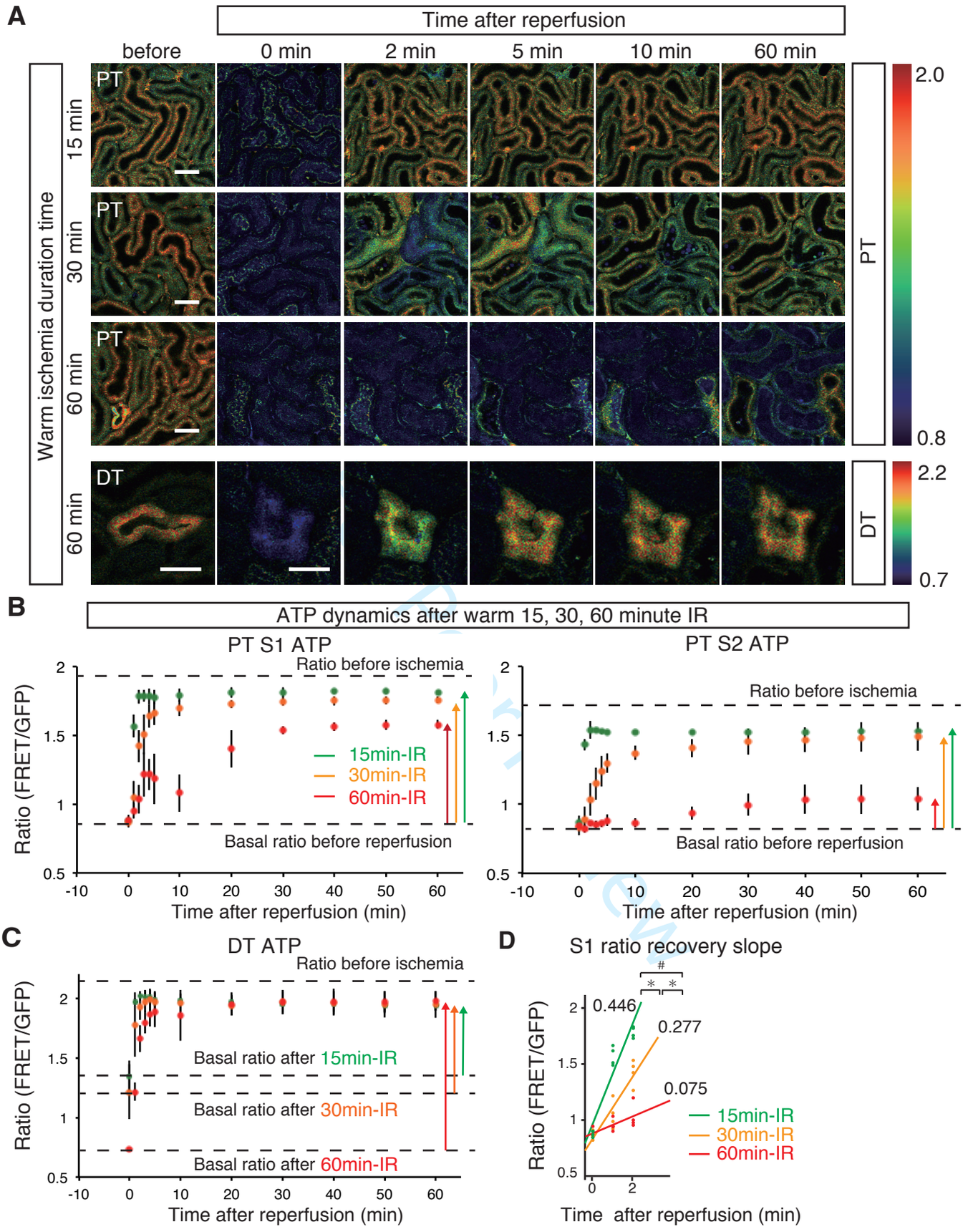

Figure 3. While ATP recovery in PTs after reperfusion varied depending on the length of ischemia, ATP recovery in DTs was quickly restored irrespective of ischemia duration. (**A**) Ratio images of PTs during reperfusion after warm 15, 30, and 60-minute ischemia, and those of DTs after warm 60-minute ischemia. (**B**) Ratio graphs of S1 and S2 PTs during reperfusion after 15, 30, and 60-minute ischemia (green, orange, and red) (n = 4 mice per group). The longer ischemic time resulted in slower and poorer recovery of ATP levels in PTs. (**C**) Ratio graphs of DTs during reperfusion after 15, 30, and 60-minute ischemia (green, orange, and red) (n = 4 mice per group). Note that the basal ratios after ischemia varied depending on ischemia time as shown in Figure 2D. Compared to those of PTs, the ratio in DTs recovered more quickly and almost completely even after 60-minute IR. (**D**) The graph of S1 ratio recovery slopes after warm15, 30, 60 minute-IR. The longer ischemic time resulted in slower recovery slopes. Multiple group comparisons were performed using ANCOVA. $^{*}P < 0.001$, $^{\#}P < 0.05$. Scale bars: (**A**) 50 μm in images of PTs and DTs.

Figure 4

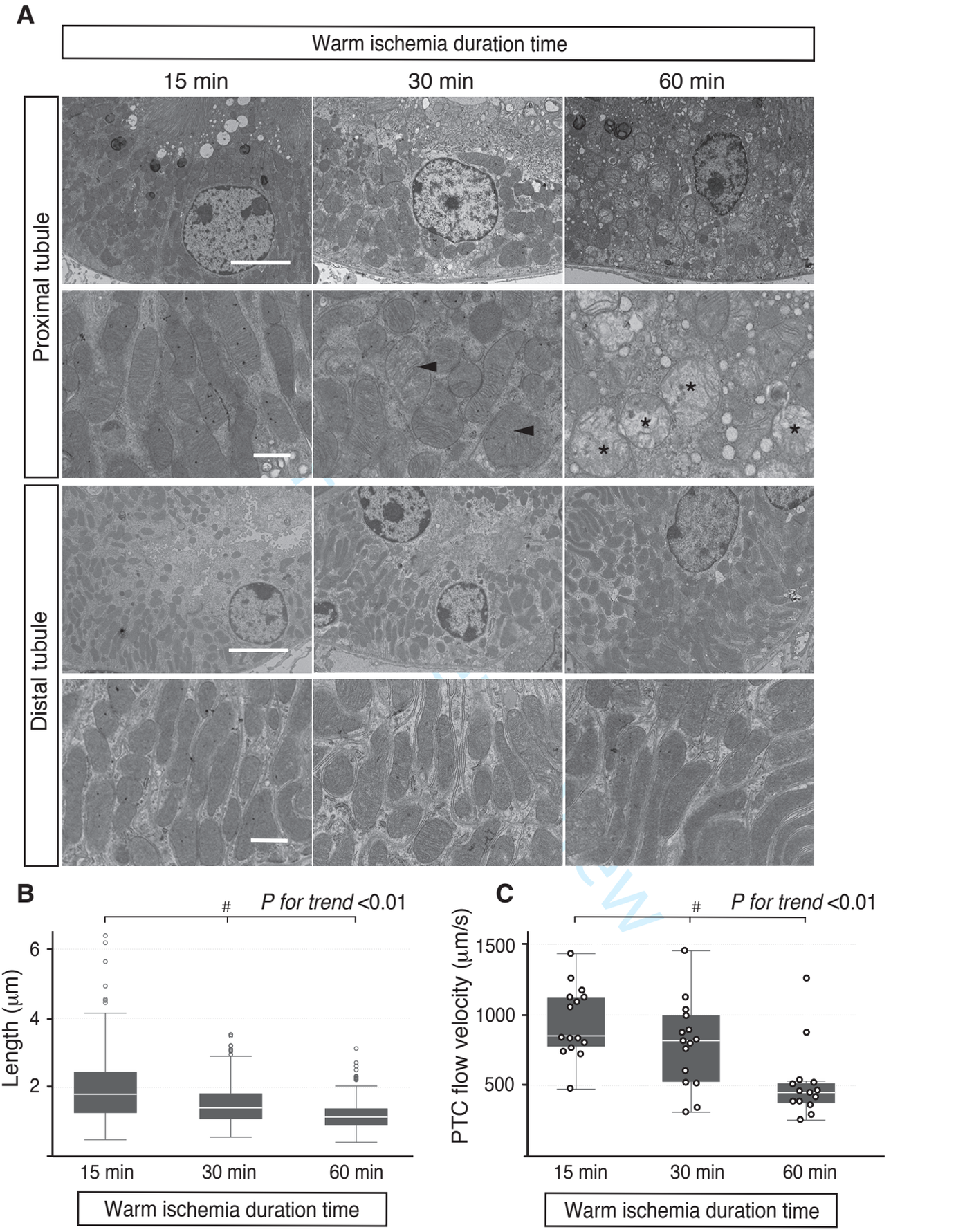

Figure 4. Mitochondrial structural changes and PTC flow velocities after warm15, 30, 60 minute-IR. (**A**) Electron microscopic analysis of the kidney 5 minutes after the induction of reperfusion after 15, 30, and 60 minute-ischemia. Mitochondrial swelling (arrowhead) and fragmentation were observed in PTs after 30 and 60 minute-IR, and the loss of cristae was additionally observed after 60 minutes-IR (asterisk). In contrast, no obvious fragmentation of mitochondria was observed in DTs even after 60 minute-IR. Scale bars: 5 μm (upper images in both PTs and DTs) and 1 μm (lower images in both PTs and DTs). (**B**) The longer ischemic time resulted in the decrease of length of mitochondria (n = 3 mice, 9 tubules, 300 mitochondria). (**C**) The longer ischemic time resulted in the slower PTC flow velocities (n = 3 mice, 15 areas). Statistical significance was assessed in Figure 5B and 5C by the nonparametric test for trend across 15, 30, and 60 minute warm IR groups and ANOVA. $^{\#}P$ *for trend* < 0.01.

Figure 5

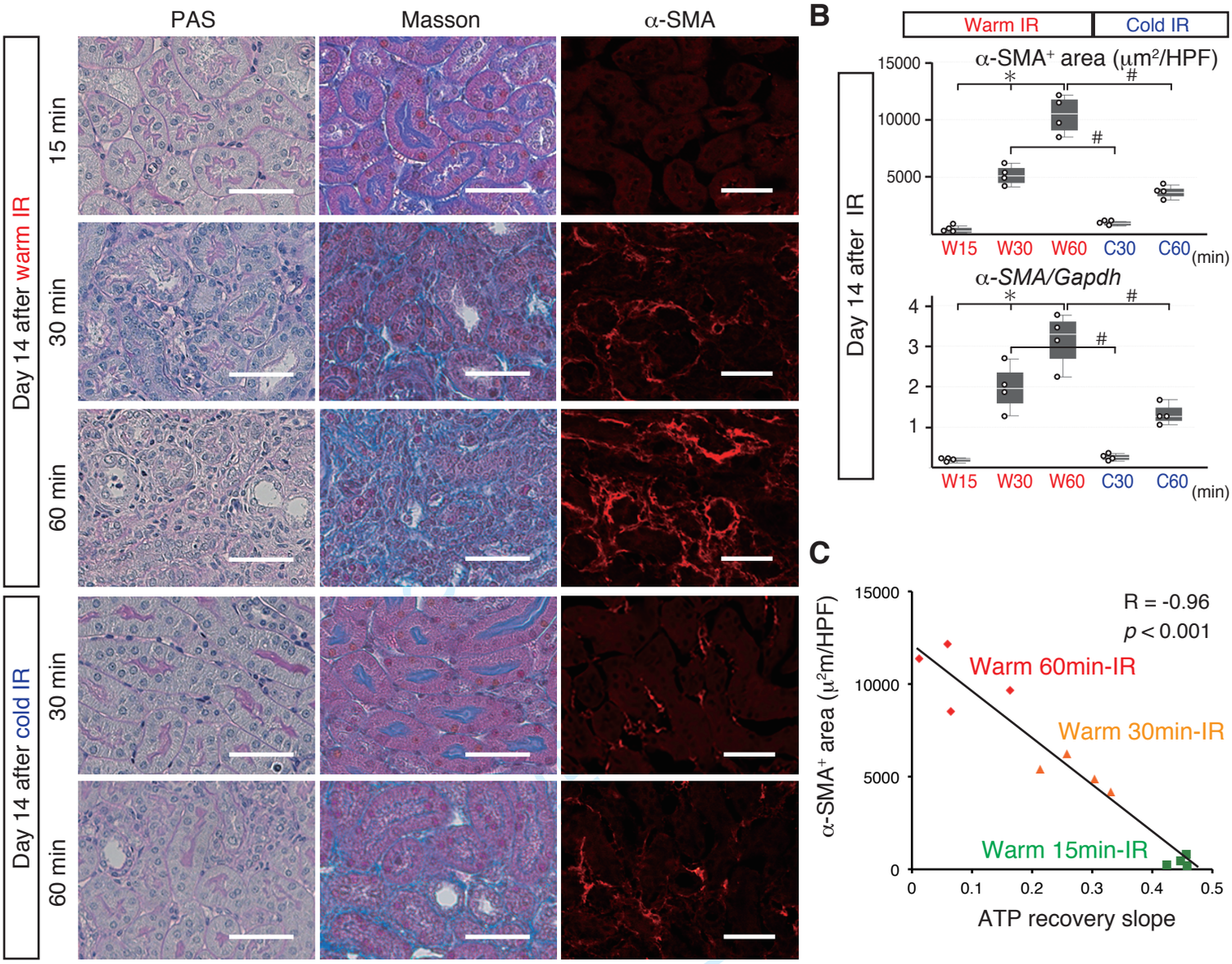

Figure 5. Fibrosis in chronic phase was inversely correlated well with the ATP recoveries in acute phase. (**A**) PAS and Masson staining of the kidneys 14 days after warm 15, 30, and 60 minute-IR and cold 30 and 60 minute-IR, and immunofluorescence analysis of α–smooth muscle actin (α-SMA). (**B**) Quantitative analysis of α-SMA in the kidneys harvested 14 day after IR. The quantitative analysis of α-SMA positive area and the expression of *α-SMA* mRNA in the kidneys harvested 14 days after IR (n = 4 mice per group). The expression levels of α-*SMA* mRNA were normalized to those of *Gapdh* mRNA. Statistical significance was assessed by the nonparametric test for trend across 15, 30, and 60 minute warm IR groups. $^{*}P$ *for trend* < 0.01. Differences between the two groups (warm 30 minute-IR vs cold 30 minute-IR, and warm 60 minute-IR vs cold 60 minute-IR) were compared using Student's *t*-test. $^{\#}P < 0.01$. These graphs showed the progression of renal fibrosis after longer warm ischemia as well as the amelioration of renal fibrosis after cold IR. (**C**) Graph showing that the fibrosis area in chronic phase was inversely correlated with S1 PTs ratio recovery slopes in acute phase. The correlation was determined by Pearson's correlation analysis. Scale bars: (**A**) 50 μm.

38 **Figure 6**

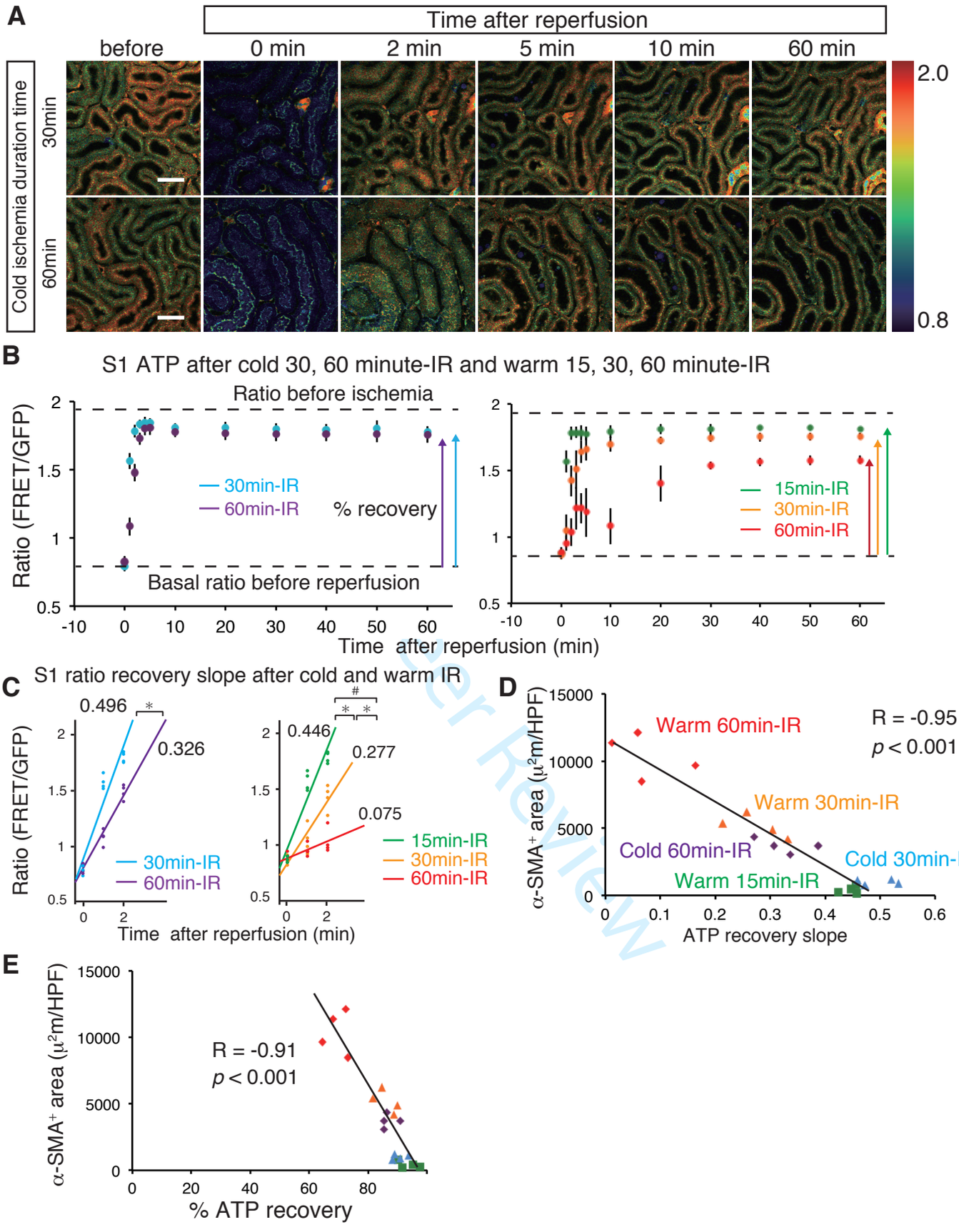

39 # Figure 6

Figure 6. Renal hypothermia improved the ATP recoveries in acute phase and the fibrosis in chronic phase after IR injury.(**A**) Ratio images of PTs during cold 30 and 60-minute IR. (**B**) Ratio graphs of PTs S1 during cold 30 and 60 minute-IR (blue and purple) (n = 4 per group). Cold ischemia improved the ATP recovery dramatically. Ratio graphs during warm IR (Figure 3B) were presented again for comparison. (**C**) The graph of ratio recovery slopes in cold 30 and 60 minute-IR. Two group comparisons were performed using ANCOVA. $^{*}P < 0.01$. The graph of ratio recovery slopes in warm IR (Figure 3D) was presented again for comparison.(**D** and **E**) Graphs demonstrated that the fibrosis area was inversely correlated well with the ratio recovery slope and % ratio recovery in acute phase. The correlation was determined by Pearson's correlation analysis. Graphs demonstrated that the fibrosis area was inversely correlated well with the ratio recovery slopes (**D**) and % ratio recovery (**E**) in acute phase. The data of warm IR in (**D**) were the same with those shown in Figure 5C, but analyzed again with the data of cold IR to show that the correlation was well maintained even when kidney samples treated with warm and cold ischemia were evaluated together. The correlation was determined by Pearson's correlation analysis. Scale bars: (**A**) 50 μm.

SUPPLEMENTARY APPLEDIX FOR THE STUDY:

Spatiotemporal ATP dynamics during acute kidney injury predicts renal prognosis

Supplementary material table of contents

Supplemental Figure 1

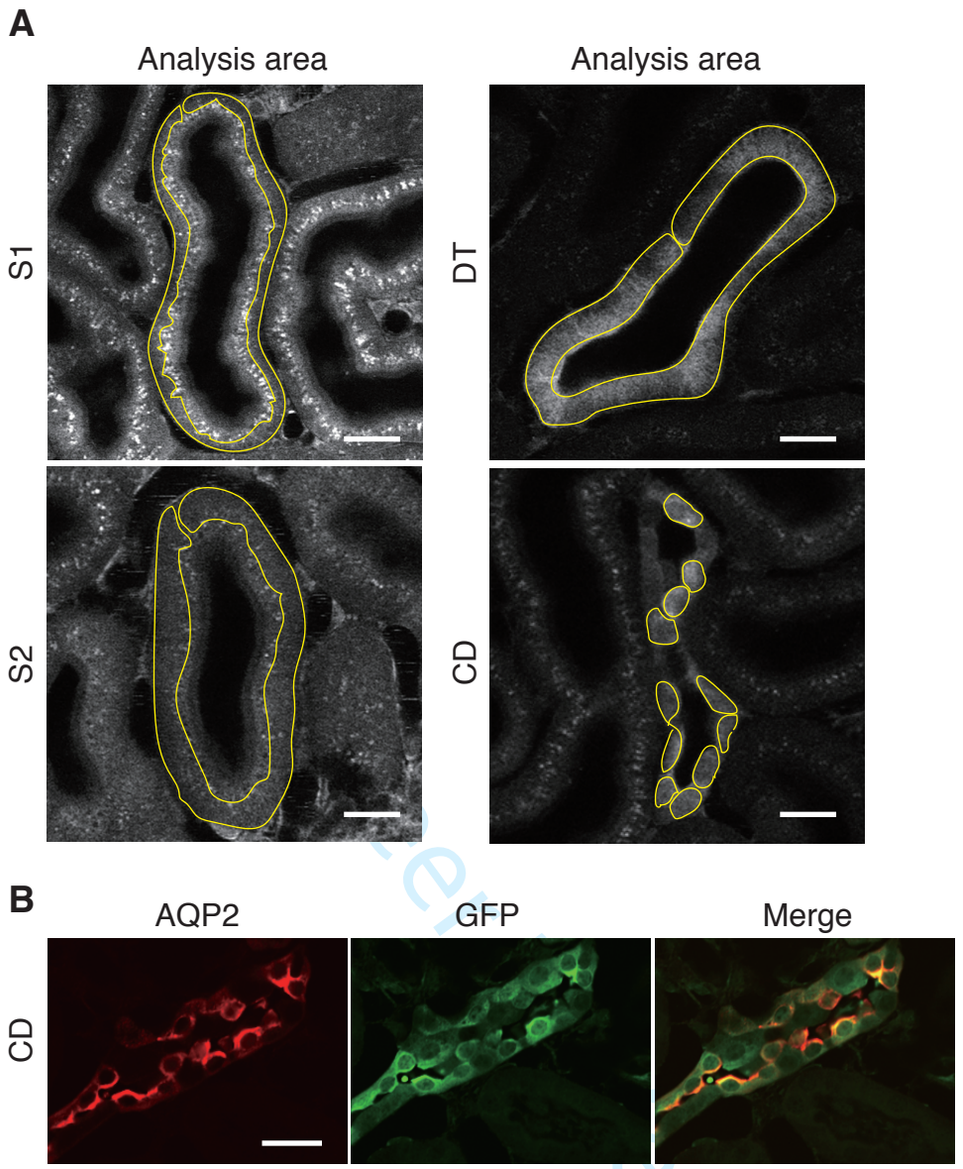

Supplemental Figure 1. Areas analyzed in monitoring ratios (A), and immunostaining of AQP2 and GFP in the collecting duct of GO-ATeam2 mice (B).

(**A**) The areas surrounded by yellow line were analyzed in monitoring ratios in each segment. The apical lumen especially in S1 PTs was omitted to exclude high autofluorescence signals. (**B**) Immunostaining of AQP2 and GFP in the kidneys of GO-ATeam2 mice demonstrating that the cells with strong expression of GO-Ateam in CDs are mainly principal cells. Scale bars: (**A** and **B**) 20 μm.

Supplemental Figure 2

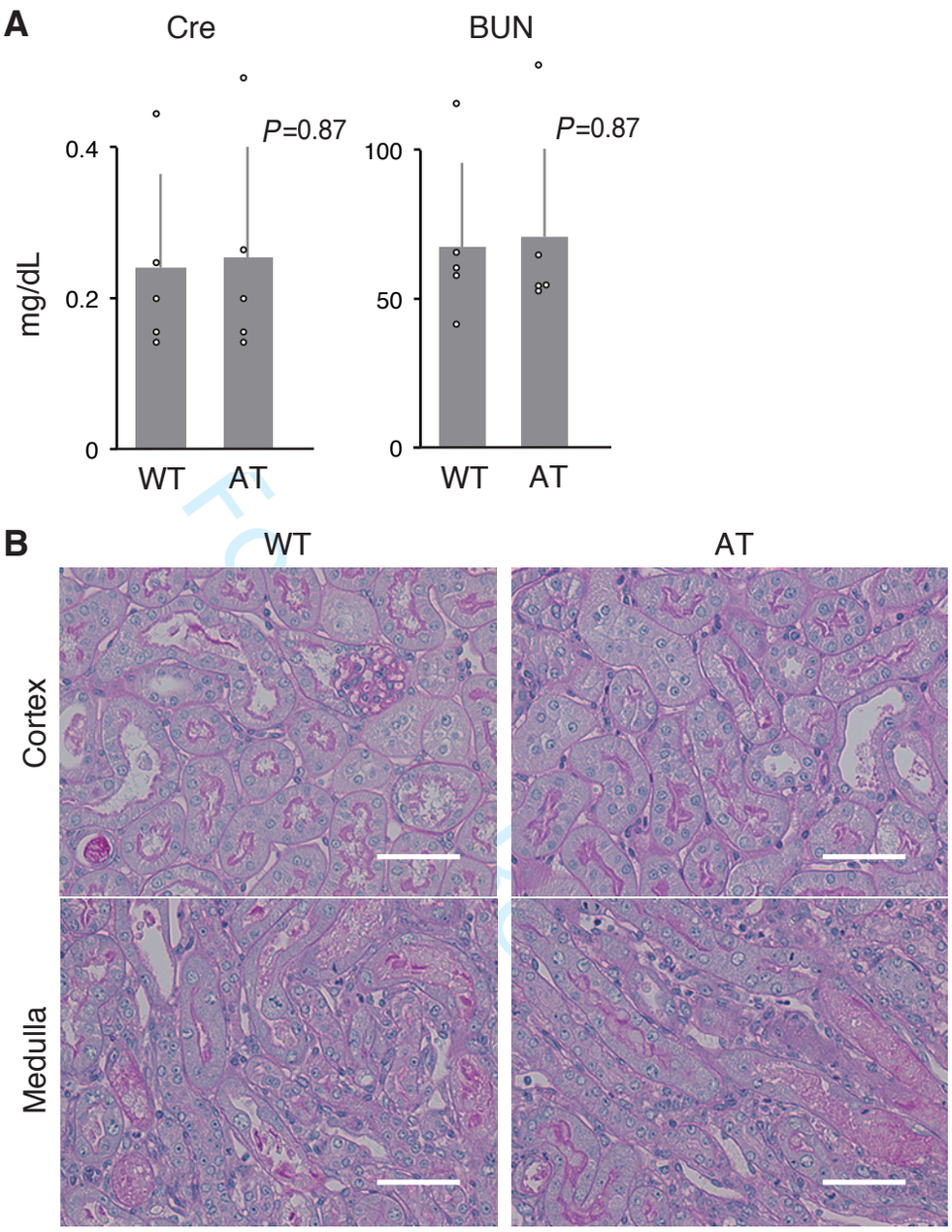

Supplemental Figure 2. Kidney function and histological alterations of wild-type and GO-ATeam2 mice after IR injury.

(**A**) Serum creatinine and BUN of wild-type (WT) and GO-ATeam2 mice two days after unilateral warm 23 minute-ischemia reperfusion (IR) with contralateral nephrectomy three days before IR (n = 5 mice per group). There was no statistically significant difference between groups. Statistical significance was assessed by Student's *t*-test. (**B**) Representative images of Periodic acid-Schiff (PAS) staining of WT and GO-Ateam2 kidneys harvested at the same time point. The severity of kidney injury was comparable between groups. Scale bars: (**B**) 50 μm.

Supplemental Figure 3

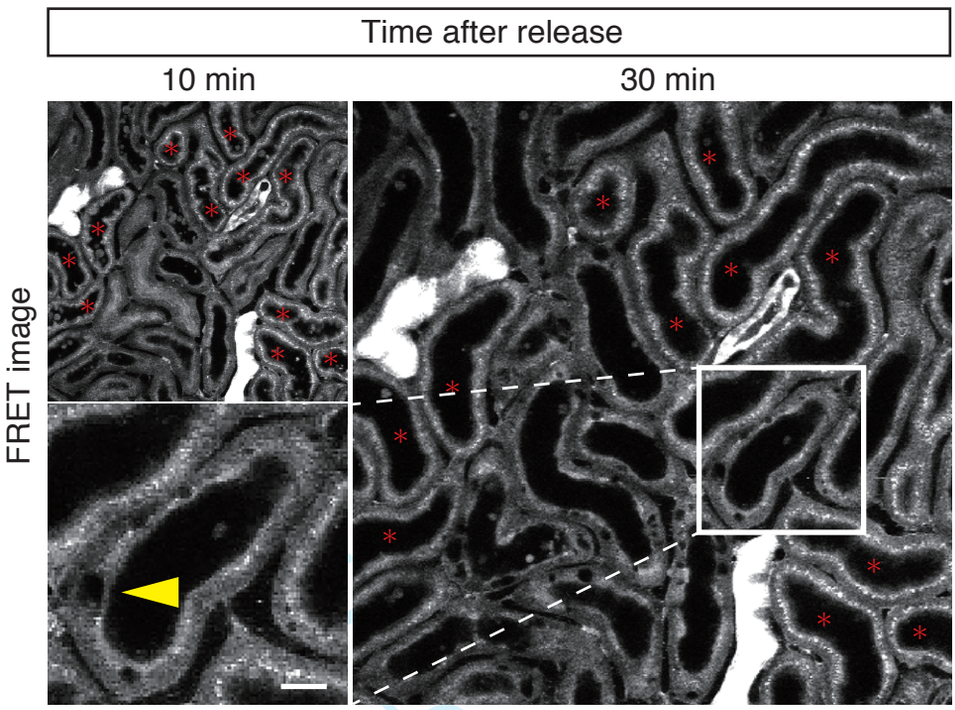

Supplemental Figure 3. Vacuolization in S2 PTs after reperfusion.
Images of FRET signals after warm 30-minute IR showing that vacuolization in S2 PTs, but not in S1 PTs with high apical autofluorescence (asterisk). Inset is showing higher magnification of vacuolization (arrowhead). Scale bars: 20 μm.

Supplemental Figure 4

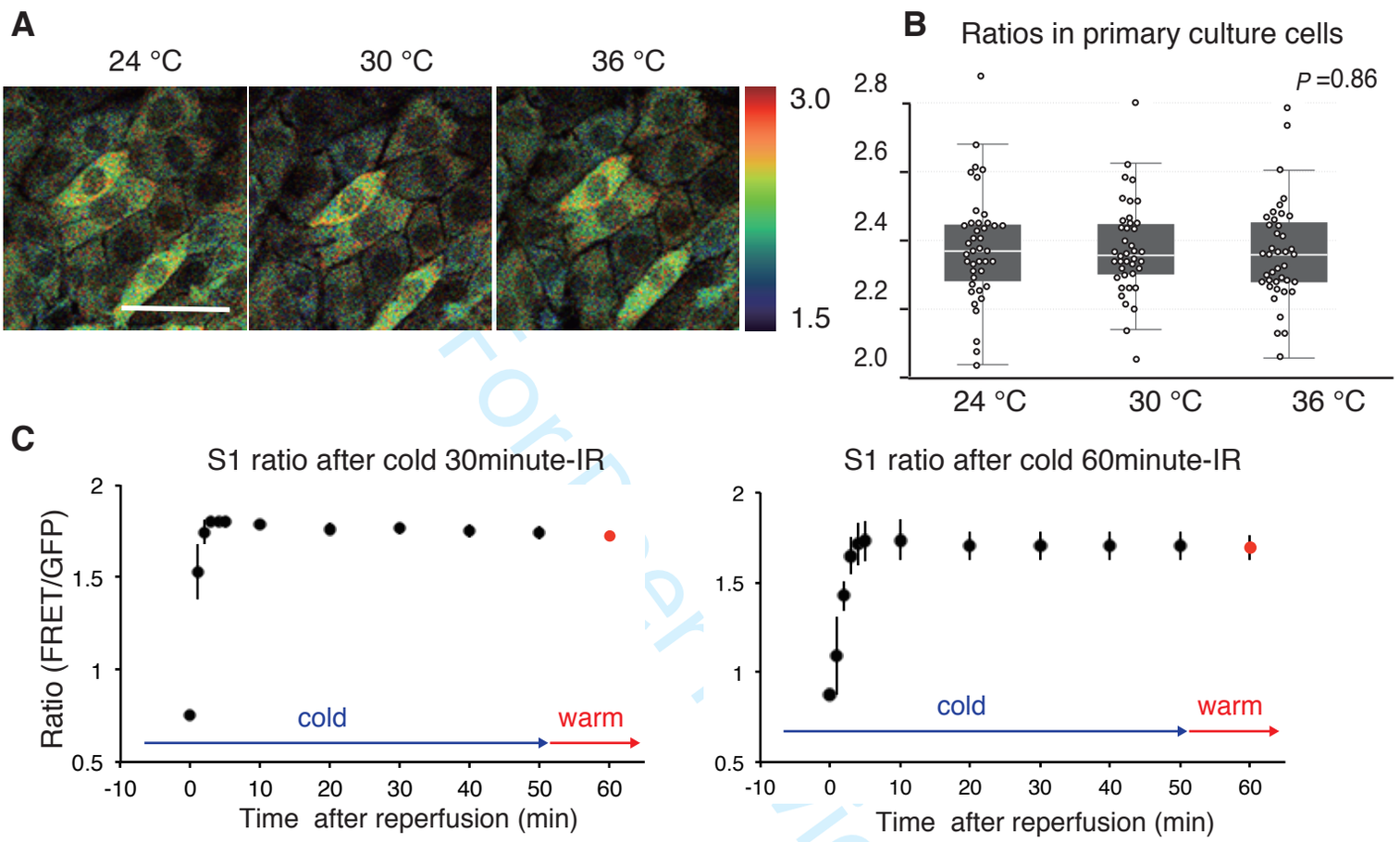

Supplemental Figure 4. Analysis of FRET ratios at different temperatures in vitro (A) and in vivo (B).

(**A**) Ratio images of renal primary culture cells from the kidneys of GO-ATeam2 mice sequentially cultured under 24, 30, and 36 °C, showing similar ratios between groups. (**B**) Ratios were similar between groups, and there was no statistically significant difference. Statistical significance was assessed by ANOVA. $^{*}P = 0.86$ (**C**) Ratio graphs of PT S1 during cold 30 and 60 minute-IR, whose kidneys were warmed 50 minutes after reperfusion, showing that the temperature did not affect the ratio *in vivo* (n = 3 per group). Scale bars: (**A**) 50 μm.

A

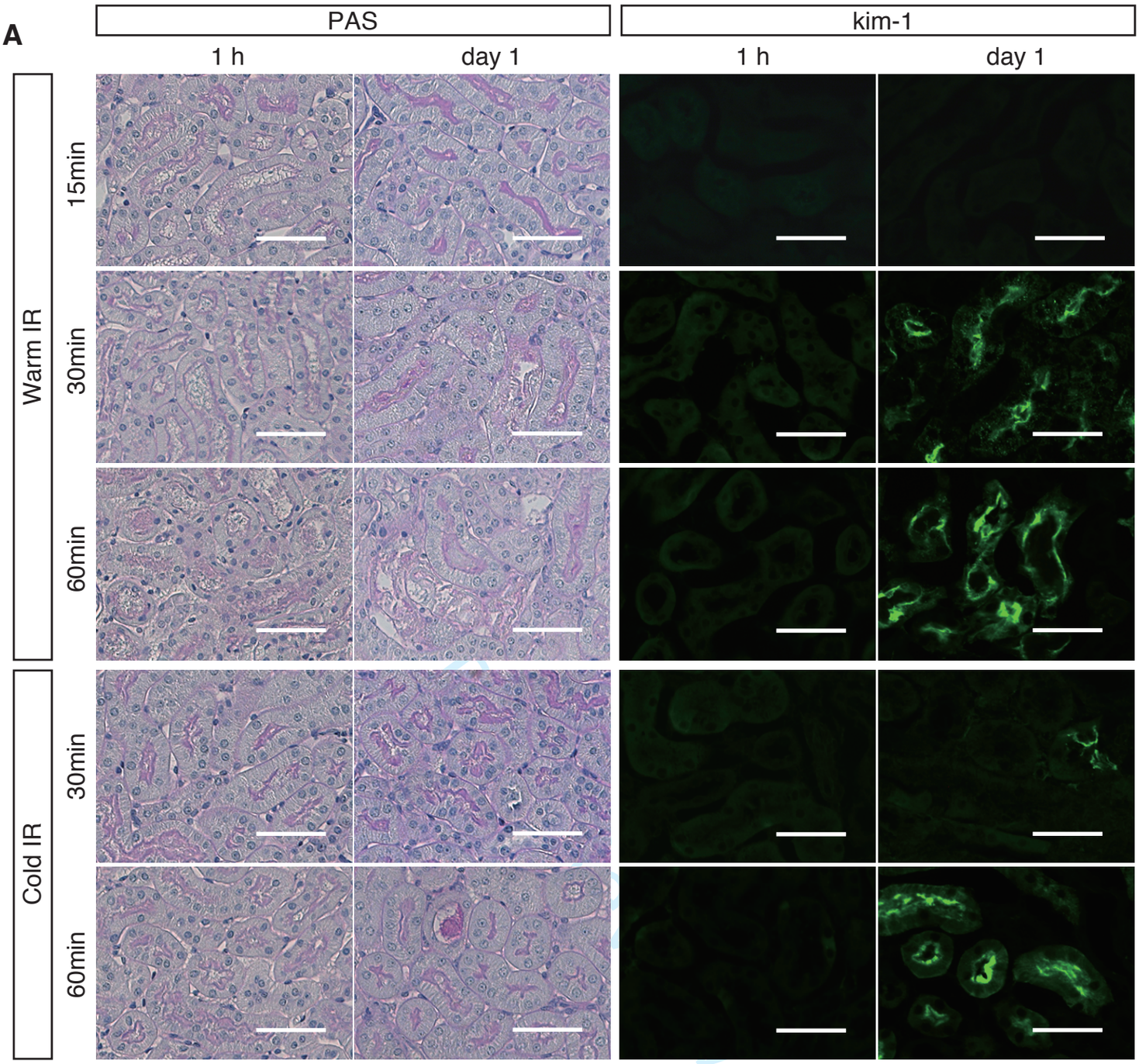

B

IR day 1 PAS scoring

	Warm			Cold	
	15min IR	30min IR	60min IR	30min IR	60min IR
Grade 0	6	1	0	4	0
Grade 1	4	2	2	7	1
Grade 2	5	9	1	4	12
Grade 3	0	3	1	0	2
Grade 4	0	0	11	0	0

Supplemental Figure 5. Histological analysis of the kidneys one hour and one day after the induction of reperfusion.

(**A**) Histological analysis of acute kidney injury after IR. Periodic acid-Schiff (PAS) staining and immunostaining of Kim-1 of the kidneys harvested one hour, and one day after the induction of reperfusion after warm 15, 30, and 60 minute-ischemia and cold 30 and 60 minute-ischemia. In the kidney harvested one hour after the induction of reperfusion, neither obvious histological injury nor the expression of Kim-1 was observed even in the kidneys treated with warm 60 minute-ischemia. (**B**) Pathological scores of acute kidney injury in the kidneys harvested one day after warm 15, 30, and 60 minute-IR and cold 30 and 60 minute-IR. Five high-power fields in the cortex per each mouse were viewed and graded for tubular injury defined as tubular necrosis, tubular dilation, casts, brush border loss (0 = 0-1%, 1 = > 1-10%, 2 = 10-25%, 3 = > 25-50%, and 4 = > 50%) (n = 3 mice per group). All scoring was performed in a blind fashion by experienced nephrologists. Scale bars: (**A**) 50 μm.

Supplemental Figure 6

A

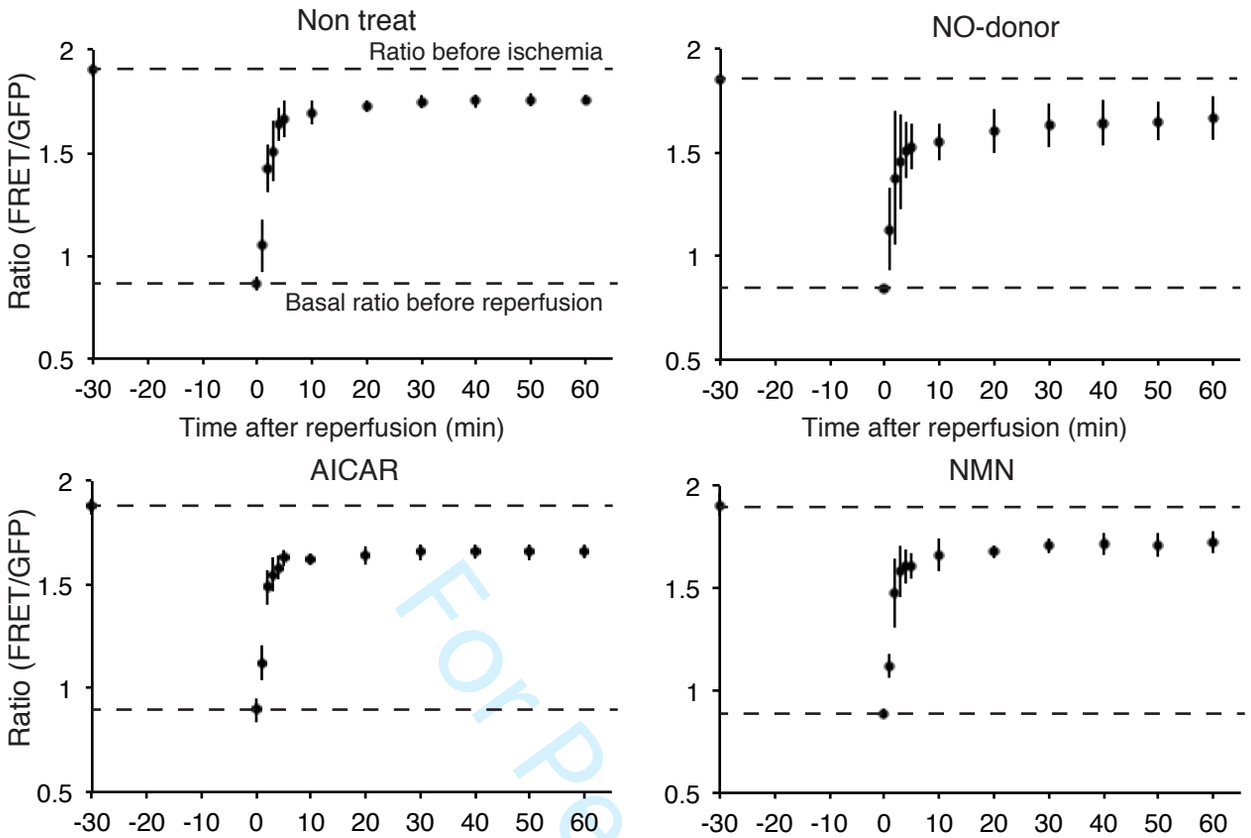

B

	Ratio before IR/*P* value (vs NT)
NT	1.90 ± 0.032/ ---
NO-donor	1.85 ± 0.016/ 0.052
AICAR	1.88 ± 0.036/ 0.360
NMN	1.91 ± 0.056/ 0.844
	Recovery slope/*P* value (vs NT)
NT	0.277 ± 0.050/ ---
NO-donor	0.266 ± 0.155/ 0.884
AICAR	0.297 ± 0.017/ 0.730
NMN	0.295 ± 0.095/ 0.767
	% recovery/*P* value (vs NT)
NT	86.2 ± 3.8/ ---
NO-donor	82.1 ± 9.5/ 0.461
AICAR	82.0 ± 4.0/ 0.039*
NMN	81.9 ± 10.1/ 0.120

Supplemental figure 6. ATP dynamics after warm 30 minute-IR treated with NO-donor, AICAR, or NMN

(**A**) Ratio graphs of PTs S1 during reperfusion after warm 30-minute ischemia with NO-donor (n = 3 mice), AICAR (n = 3 mice), and NMN (n = 3 mice). None of compounds could elevate the ratio before IR and the ratio % recovery. (**B**) Table of each ratio before IR, recover slope, % recover, and *P* value. Differences between the groups (NT vs NO-donor / AICAR / NMN) in the ratio before IR and the % recovery were compared using Student's *t*-test. Those in the recovery slope were compared using ANCOVA. $^{*}P < 0.05$